

# MVP-LAM: Learning Action-Centric Latent Action via Cross-Viewpoint Reconstruction

Jung Min Lee<sup>1</sup> Dohyeok Lee<sup>1</sup> Seokhun Ju<sup>1</sup> Taehyun Cho<sup>1</sup> Jin Woo Koo<sup>1</sup> Li Zhao<sup>2</sup> Sangwoo Hong<sup>3</sup>  
Jungwoo Lee<sup>1,4</sup>

## Abstract

Learning *latent actions* from diverse human videos enables scaling robot learning beyond embodiment-specific robot datasets, and these latent actions have recently been used as pseudo-action labels for vision-language-action (VLA) model pretraining. To make VLA pretraining effective, latent actions should contain information about the underlying agent’s actions despite the absence of ground-truth labels. We propose Multi-ViewPoint Latent Action Model (**MVP-LAM**), which learns discrete latent actions that are highly informative about ground-truth actions from time-synchronized multi-view videos. MVP-LAM trains latent actions with a *cross-viewpoint reconstruction* objective, so that a latent action inferred from one view must explain the future in another view, reducing reliance on viewpoint-specific cues. On Bridge V2, MVP-LAM produces more action-centric latent actions, achieving higher mutual information with ground-truth actions and improved action prediction, including under out-of-distribution evaluation. Finally, pre-training VLAs with MVP-LAM latent actions improves downstream manipulation performance on the SIMPLER and LIBERO-Long benchmarks.

## 1. Introduction

Collecting real-world robot demonstrations remains a central bottleneck in training generalist manipulation policies (McCarthy et al., 2024). Unlike foundation models in other domains, robot learning is constrained by the cost of acquiring action-labeled trajectories, which typically requires human teleoperation. This makes large-scale data collection slow and expensive, and the resulting datasets

<sup>1</sup>Seoul National University, Seoul, South Korea <sup>2</sup>Microsoft Research Asia, Beijing, China <sup>3</sup>Konkuk University, Seoul, South Korea <sup>4</sup>HodooAI Labs, Seoul, South Korea. Correspondence to: Jungwoo Lee <jungleee@snu.ac.kr>.

Preprint. February 4, 2026.

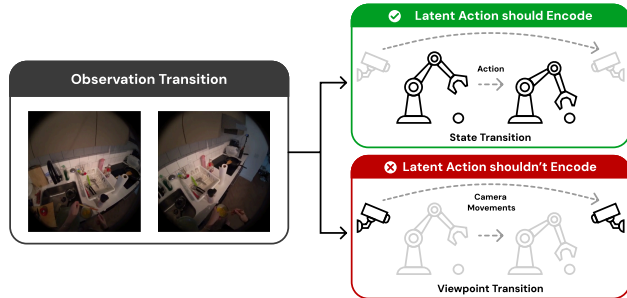


**Figure 1. Why viewpoint variation interferes with learning latent actions.** Viewpoint variation acts as noise. Frame-to-frame visual differences reflect both interaction-driven state changes and viewpoint-dependent appearance changes (e.g., camera movements). Because these factors are entangled, the same underlying action can induce different visual transitions across viewpoints. This confounding makes it difficult to learn latent actions that are consistently predictive of the underlying control actions.

often depend on a specific embodiment and sensor setup. To alleviate this limitation, learning from video (LfV) has emerged as a promising alternative that exploits abundant human manipulation videos to acquire transferable priors over manipulation-relevant dynamics. A fundamental challenge, however, is that such videos do not provide low-level robot action labels, preventing standard supervised imitation learning.

To address missing actions, recent methods learn *latent actions*, compact representations of video frame transitions, and use them as pseudo-action labels (Ye et al., 2024; Chen et al., 2024b; Bu et al., 2025; Kim et al., 2025a; Chen et al., 2025b). A latent action model (LAM) learns such representations from unlabeled videos by encoding frame-to-frame transitions and optimizing a reconstruction loss to predict the next observation from the current observation and the latent action. These pseudo-labels have been used to pre-train vision-language-action (VLA) models and to define reusable skills for downstream control.

For effective VLA pretraining, the key requirement is that latent actions remain strongly informative about the underlying actions even when ground-truth actions are unavailable.

Motivated by this, we define an *action-centric latent action* as one that preserves high mutual information (MI) with the true action.

A key obstacle for action-centric latent actions is *exogenous noise*, where visual transitions can be spuriously influenced by factors other than the agent’s actions yet still correlate with frame-to-frame changes, e.g., people moving in the background (Misra et al., 2024; Nikulin et al., 2025b). Among these factors, we focus on viewpoint variation. Viewpoint changes introduce camera movements and perspective shifts, entangling visual transitions with the agent’s action. As a result, latent actions learned from single-view reconstruction can overfit to viewpoint-dependent cues and become less predictive of the actions.

We propose **Multi-ViewPoint Latent Action Model** (MVP-LAM), which learns discrete latent actions that are highly informative about ground-truth actions. MVP-LAM is trained on time-synchronized multi-view videos with a *cross-viewpoint reconstruction* objective, where a latent action inferred from one view is used to predict the future observation in another view. This discourages latent actions from encoding the viewpoint-specific information and achieves more action-centric latent actions.

Empirically, MVP-LAM learns more action-centric latent actions than LAMs trained on single-view data with pixel-reconstruction objectives. On Bridge V2 (Walke et al., 2023), MVP-LAM achieves higher mutual information between latent actions and ground-truth actions and enables better action prediction accuracy with a simple single linear layer, including under out-of-distribution (OOD) datasets. Finally, VLAs pretrained with MVP-LAM latent actions outperform baselines on the SIMPLER (Li et al., 2024) and LIBERO-Long (Liu et al., 2023) benchmarks.

Our contributions are summarized as follows:

1. We introduce MVP-LAM, a discrete latent action model trained from time-synchronized multi-view videos with a cross-viewpoint reconstruction objective, where a latent action inferred from one view is used to predict the future observation in another view.
2. We show that MVP-LAM achieves the highest mutual information with ground-truth actions over baselines and improves action prediction on Bridge V2, including under out-of-distribution evaluation. This improvement is achieved without action supervision during latent action learning and without relying on the performance of off-the-shelf models.
3. We demonstrate the effectiveness of MVP-LAM latent actions as pseudo-labels for VLA pretraining, shown by improvement of the downstream manipulation performance on SIMPLER and LIBERO-Long.

## 2. Related Works

**Latent Action Learning from Video.** Recent progress in video-based robot learning has studied how to extract useful representations from large-scale human demonstration videos for downstream control. Several works learn video priors such as object affordances or trajectories (Bharadhwaj et al., 2023; Bahl et al., 2023; Bharadhwaj et al., 2024; Wen et al., 2023), while another line learns latent actions as an abstraction of temporal transitions by modeling frame-to-frame visual dynamics without action supervision (Schmidt & Jiang, 2024; Ye et al., 2024; Bruce et al., 2024; Chen et al., 2024b; Bu et al., 2025; Chen et al., 2025a;b; Wang et al., 2025). Among these works, LAPA (Ye et al., 2024) and Moto (Chen et al., 2024b) extract latent actions from unlabeled videos and use them as scalable supervision for training downstream visuomotor policies. In addition, Genie (Bruce et al., 2024), IGOR (Chen et al., 2025a), and CoLA-World (Wang et al., 2025) incorporate latent actions into world models (Ha & Schmidhuber, 2018), improving controllable video generation and supporting downstream embodied planning and manipulation. In contrast, Uni-VLA (Bu et al., 2025) focuses on improving the latent action quality for effective downstream policy training by using language descriptions or additional structural objectives in latent action training.

Prior latent action approaches study the latent action learning with single-view video, but to our knowledge, none of them explicitly use multi-view video during LAM training. MVP-LAM uses cross-viewpoint reconstruction on multi-view data to construct action-centric latent actions.

**Learning from Videos with Diverse Viewpoints.** In robot learning, learned policies often exhibit poor generalization across viewpoints due to limited viewpoint diversity in open-source robot datasets (Chen et al., 2024a). One line of work mitigates such limitations via 3D-aware representations (e.g., point cloud) or data augmentation with novel-view synthesis (NVS) (Driess et al., 2022; Shim et al., 2023; Zhu et al., 2023; Goyal et al., 2023; Ze et al., 2024; Hirose et al., 2022; Tian et al., 2024). Viewpoint variation is, however, prevalent in real-world manipulation videos, especially in egocentric data (e.g., EgoExo4D (Grauman et al., 2024)), and can serve as a scalable source of viewpoint diversity. Accordingly, R3M (Nair et al., 2022) and HRP (Srirama et al., 2024) pretrain visual representations on large-scale egocentric human videos and show improved robustness of downstream policies under viewpoint changes.

These methods primarily aim at observation representations and often require additional components such as camera calibration, dense multi-view coverage of the same scene, or computationally expensive 3D reconstruction and neural rendering.

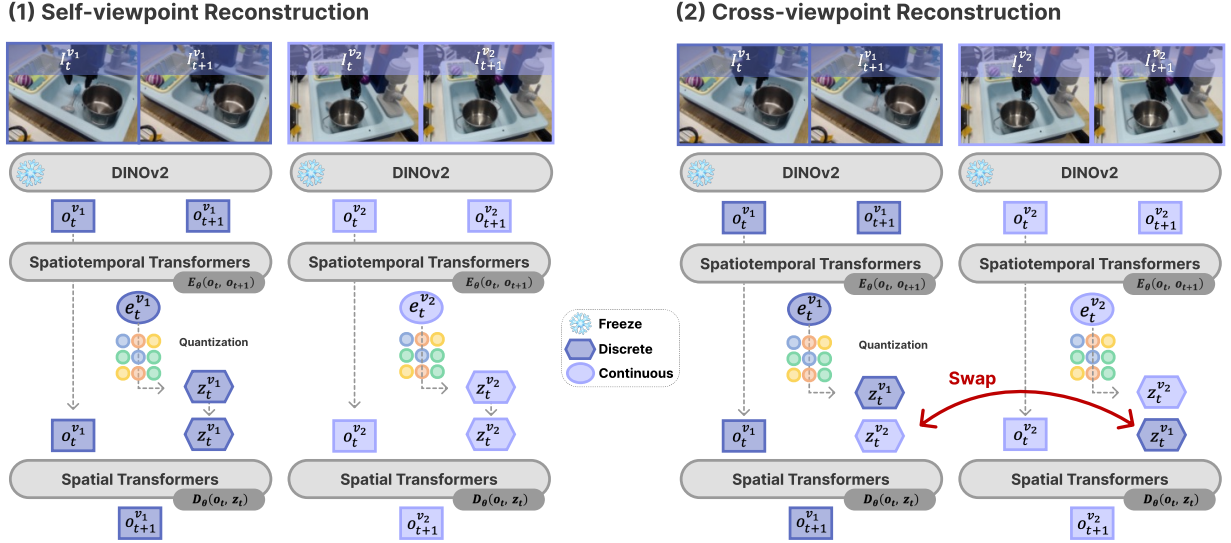


**Figure 2. MVP-LAM training with time-synchronized multi-view videos.** (1) *Self-viewpoint reconstruction* (left): for each view  $v$ , frozen DINOv2 extracts features  $(o_t^v, o_{t+1}^v)$ . A spatiotemporal encoder produces a continuous latent  $e_t^v$  that is vector-quantized into a discrete token  $z_t^v$ , and a decoder reconstructs  $o_{t+1}^v$  from  $(o_t^v, z_t^v)$ . (2) *Cross-viewpoint reconstruction* (right): MVP-LAM swaps latent tokens across views (e.g.,  $z_t^{v1} \leftrightarrow z_t^{v2}$ ) while reconstructing each view’s future feature, encouraging  $z_t$  to capture inherent transition information.

**Exogenous Noise in Latent Action Learning.** Exogenous noise in real-world datasets can hinder reliable latent action learning. In the presence of such non-i.i.d. noise, learning representations that include the minimal information necessary to control the agent from videos can require exponentially more samples than learning from action-labeled trajectories (Misra et al., 2024). In addition, such noise can dominate observation transitions and incentivize LAMs to encode it (Nikulin et al., 2025b), and, theoretically, even linear LAMs tend to capture the dominant variation, which may include the noise (Zhang et al., 2025). To mitigate this issue, LAOM (Nikulin et al., 2025b) incorporates a small amount of action supervision to guide the latent actions. Other approaches reduce the influence of the distractors without action labels, for example, by learning object-centric representations via slot decomposition (Klepach et al., 2025) or by asking vision-language models (VLM) to ignore distractors (Nikulin et al., 2025a).

While these methods provide insights for reducing the noise, they introduce additional dependencies, such as action labels, reliable object decomposition, or the quality of pre-trained VLMs. In addition, their evaluations are often limited to controlled benchmarks with synthetic distractors (e.g., Distracting Control Suite), leaving open questions about how these methods translate to realistic, noisy manipulation data and whether they yield consistent gains in multi-task or long-horizon settings.

### 3. Method

We propose **MVP-LAM**, a latent action model trained with time-synchronized multi-view videos and a cross-viewpoint reconstruction objective, which produces discrete latent actions as *pseudo-labels* for training VLA models from unlabeled videos.

#### 3.1. Problem Formulation

We denote a video by a sequence of images  $\{I_t\}_{t=1}^T$ . For each timestep  $t$ , we assume that the image  $I_t$  is generated under a camera pose  $v_t$ . For each image  $I_t$ , we extract a visual observation in a feature space as  $o_t = f(I_t)$ , where  $f(\cdot)$  is a visual encoder such as DINOv2 (Oquab et al., 2024) or MAE (He et al., 2022). Since video datasets may have different frame rates, we define a fixed temporal stride  $H$  and set  $o_{t+1} = f(I_{t+H})$ .

**Latent action model.** LAM is generally implemented as a vector-quantized variational autoencoder (VQ-VAE) (van den Oord et al., 2017), with VLA training in mind. LAM learns a latent action  $z_t$  that summarizes the transition from  $o_t$  to  $o_{t+1}$ . Concretely, an encoder produces a continuous latent  $e_t = E_\theta(o_t, o_{t+1})$ , which is vector-quantized into a codebook entry, i.e.,  $z_t = \text{Quantize}(e_t)$ . A decoder then predicts the next observation feature as  $\hat{o}_{t+1} = D_\theta(o_t, z_t)$ . In standard LAM training, the decoder

does not take the viewpoint  $v_t$  as input. The training objective is

$$\mathcal{L}_\theta(o_t, o_{t+1}) = \|o_{t+1} - \hat{o}_{t+1}\|_2^2 + \mathcal{L}_{\text{quant}} + \mathcal{L}_{\text{commit}}, \quad (1)$$

where  $\mathcal{L}_{\text{quant}}$  and  $\mathcal{L}_{\text{commit}}$  are the standard VQ-VAE quantization and commitment losses:

$$\begin{aligned}\mathcal{L}_{\text{quant}} &= \|\text{sg}[e_t] - z_t\|_2^2, \\ \mathcal{L}_{\text{commit}} &= \beta \|e_t - \text{sg}[z_t]\|_2^2\end{aligned}$$

Since  $z_t$  encodes what changes from  $o_t$  to  $o_{t+1}$ , it serves as a discrete representation of the visual transition and can be used as a pseudo-action label when ground-truth actions are unavailable. Since  $z_t$  is discrete, we can pretrain a VLM with a cross-entropy (CE) objective to predict  $z_t$ , and then use it to initialize VLA finetuning on downstream robot tasks.

### 3.2. Action-centric Latent Action

When latent actions are used as pseudo-action labels for behavior cloning policies, it is desirable that the learned latent action  $Z_t$  preserves as much information as possible about the underlying action  $A_t$ .<sup>1</sup> We denote the state by  $S_t$ , and assume an expert policy induces actions  $A_t \sim \pi^*(\cdot | S_t)$  for a given task. In the pretraining stage, we typically do not observe  $S_t$  or  $A_t$ . Instead, we only observe images (or their features)  $O_t = f(I_t)$ . LAM produces latent actions from consecutive observations, i.e.,  $Z_t = E_\theta(O_t, O_{t+1})$  (with vector quantization when using VQ-VAE).

Motivated by [Zhang et al. \(2025\)](#), we define a latent action  $Z_t$  *action-centric* if it is highly informative about the underlying action  $A_t$ . We quantify this by mutual information and consider the objective

$$\max_{Z_t} \mathcal{I}(Z_t; A_t). \quad (2)$$

In this context, viewpoint variation acts as noise. Changes in camera pose  $V_t$  can induce frame-to-frame differences in  $O_t$  that are predictive of  $Z_t$  but are not caused by the action  $A_t$ . When  $Z_t$  is learned under a limited-capacity bottleneck such as vector quantization, allocating representational capacity to viewpoint-dependent factors can come at the expense of action-relevant dynamics and reduce  $\mathcal{I}(Z_t; A_t)$ . Under simplifying assumptions detailed in [Appendix A](#), one can derive a lower bound

$$\mathcal{I}(Z_t; A_t) \geq \mathcal{H}(Z_t) - \mathcal{I}(Z_t; V_t, V_{t+1} | S_t, S_{t+1}) - C \quad (3)$$

where  $C$  is a constant independent of the latent action  $Z_t$ . This bound suggests that when  $\mathcal{H}(Z_t)$  is constrained, decreasing  $\mathcal{I}(Z_t; V_t, V_{t+1} | S_t, S_{t+1})$  can improve action-centricity. This motivates using time-synchronized multi-view videos together with a cross-viewpoint reconstruction objective to discourage viewpoint-dependent factors in  $Z_t$ .

<sup>1</sup>We use uppercase letters (e.g.,  $Z_t$ ) to denote random variables.

### 3.3. Multi-Viewpoint Latent Action Learning

Building on this motivation, we introduce MVP-LAM, which leverages time-synchronized multi-view videos and cross-viewpoint reconstruction to learn action-centric latent actions. Although single-view capture is more convenient to collect than multi-view, it remains practical at scale for human videos ([Sermanet et al., 2018](#)), and various multi-view human datasets are readily available ([Kwon et al., 2021](#); [Zheng et al., 2023](#); [Sener et al.; Grauman et al., 2024](#)). For clarity, we describe the two-view case but note that the objective extends to more views.

Given time-synchronized image pairs  $\{(I_t^{v_1}, I_t^{v_2})\}_{t=1}^T$ , we first extract visual features  $o_t^v = f(I_t^v)$  using DINOv2, producing object-centric observation features. For each viewpoint  $v \in \{v_1, v_2\}$ , the encoder  $E_\theta$  predicts a latent action from consecutive observations:

$$e_t^v = E_\theta(o_t^v, o_{t+1}^v), \quad (4)$$

$$z_t^v = \text{Quantize}(e_t^v). \quad (5)$$

As in standard LAMs, the decoder  $D_\theta$  is trained to predict the next observation from the current observation and a latent action. To reduce the effect of viewpoint variation during LAM training, MVP-LAM optimizes two complementary reconstruction terms: (i) **self-viewpoint reconstruction**, which predicts  $o_{t+1}^v$  from  $(o_t^v, z_t^v)$  within the same viewpoint, and (ii) **cross-viewpoint reconstruction**, which swaps latent actions across synchronized views and predicts  $o_{t+1}^v$  from  $(o_t^v, z_t^{\tilde{v}})$  for  $v \neq \tilde{v}$ . Formally, for two synchronized views  $\{v_1, v_2\}$ , these terms are defined as

$$\mathcal{L}_{\text{self}} = \sum_{v \in \{v_1, v_2\}} \|o_{t+1}^v - D_\theta(o_t^v, z_t^v)\|_2^2, \quad (6)$$

$$\mathcal{L}_{\text{cross}} = \sum_{\substack{v, \tilde{v} \in \{v_1, v_2\} \\ v \neq \tilde{v}}} \|o_{t+1}^v - D_\theta(o_t^v, z_t^{\tilde{v}})\|_2^2. \quad (7)$$

The full objective of MVP-LAM is

$$\mathcal{L}_{\text{MVP-LAM}} = \mathcal{L}_{\text{self}} + \mathcal{L}_{\text{cross}} + \mathcal{L}_{\text{quant}} + \mathcal{L}_{\text{commit}}. \quad (8)$$

We briefly relate cross-viewpoint reconstruction to conditional mutual information in [Equation 3](#). Reducing  $\mathcal{L}_{\text{self}}$  and  $\mathcal{L}_{\text{cross}}$  enforces  $D_\theta(o_t^v, z_t^v) \approx D_\theta(o_t^v, z_t^{\tilde{v}})$  for  $v \neq \tilde{v}$ . Since the decoder is not conditioned on the viewpoint of the latent action, any viewpoint-specific factors encoded in  $z_t^v$  would increase the cross-viewpoint reconstruction loss. Minimizing  $\mathcal{L}_{\text{cross}}$  therefore discourages  $z_t^v$  from encoding information that is specific to  $(V_t, V_{t+1})$  beyond what is determined by  $(S_t, S_{t+1})$ . Equivalently, it reduces viewpoint dependence in  $Z_t$  and thereby decreases the conditional mutual information  $\mathcal{I}(Z_t; V_t, V_{t+1} | S_t, S_{t+1})$ .

## 4. Experiments

We evaluate whether MVP-LAM learns action-centric discrete latent actions and whether these latent actions serve as effective pseudo-labels for VLA pretraining. Specifically, we address three questions: **RQ1**. Are MVP-LAM latent actions more action-centric? **RQ2**. Do they improve downstream manipulation performance after VLA finetuning? **RQ3**. Do they preserve transition-relevant information under viewpoint perturbations?

### 4.1. Experiment Setup

**Baselines.** We compare MVP-LAM against the following three representative LAMs. We provide details of the baselines in Appendix D.1.

- **UniVLA** (Bu et al., 2025) learns discrete task-relevant latent action tokens with a VQ bottleneck by encoding consecutive DINov2 features. We use UniVLA as the primary baseline because MVP-LAM is implemented as a direct modification of UniVLA.
- **LAPA** (Ye et al., 2024) discretizes observation transitions using a VQ-VAE latent action quantizer.
- **Moto** (Chen et al., 2024b) learns a latent motion tokenizer that maps videos to sequences of discrete motion tokens with a large VQ codebook.

**Implementation details.** MVP-LAM follows the UniVLA LAM architecture. For the training dataset, we use time-synchronized multi-view robot trajectories from Open X-Embodiment (OXE) (Collaboration et al., 2023), using the OpenVLA training mixture (Kim et al., 2024), and additionally include multi-view human manipulation videos from EgoExo4D (Grauman et al., 2024). Overall, the training set contains 312k trajectories and we train for 160k steps. The full data mixture and training details of MVP-LAM are provided in Appendix C.1.

### 4.2. Are MVP-LAM latent actions more action-centric?

We evaluate how action-centric a latent action is by measuring (i) mutual information between latent actions and ground-truth actions, and (ii) how well actions can be predicted from latent actions with a simple linear layer.

**Action normalization across LAMs.** Different LAMs operate at different temporal strides  $H$ . To make  $A_{t:t+H}$  comparable, we convert per-step actions into a *net relative action* over each model’s horizon by undoing the dataset-specific normalization, aggregating over the horizon, and renormalizing with original statistics. We provide the details of this process in Appendix B.

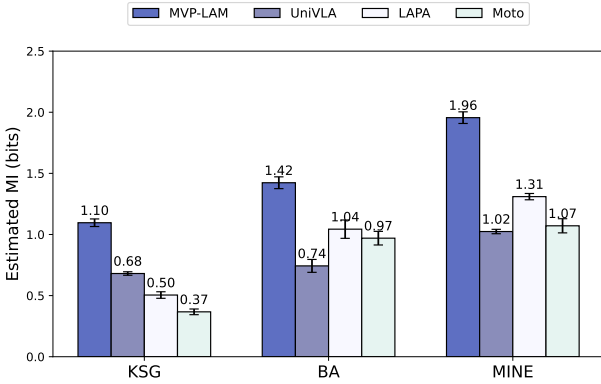


**Figure 3. Estimated mutual information.**  $\mathcal{I}(Z; A)$  on Bridge V2 with KSG, BA, and MINE estimators. For KSG, latent actions are randomly projected to  $d=256$  prior to estimation. Higher is better. Error bars show standard deviation over four seeds.

**Mutual information estimation.** On Bridge V2, we estimate  $\mathcal{I}(Z; A)$  using three estimators: the nonparametric Kraskov–Stögbauer–Grassberger (KSG) estimator, and two variational estimators (Barber–Agakov (BA) (Barber & Agakov, 2003) and a MINE style bound (Belghazi et al., 2018)). We use  $k=5$  for KSG. Since KSG is unstable in high dimensions, we apply a random projection to the latent actions so that the overall latent action dimension, including the code length, becomes  $d=256$  before KSG. We provide details of MI evaluation in Appendix B.

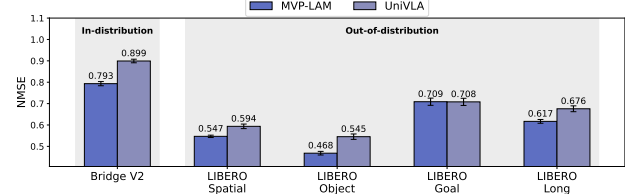


**Figure 4. Linear probing result.** NMSE of a linear layer predicting actions from latent actions. Bridge V2 is in-distribution; LIBERO (Spatial/Object/Goal/Long) is out-of-distribution. Lower is better. Error bars show standard deviation over four seeds.

**Linear probing.** To evaluate the inclusion of ground-truth actions in the latent actions, we use linear probing as Nikulin et al. (2025b). Linear probing evaluates how much information is readily accessible in a representation by fitting a simple readout model on top of frozen features (Alain & Bengio, 2017). Here, we freeze the LAM and train a lightweight probe to predict ground-truth actions from latent actions. We use a linear layer  $\hat{a}_t = Wz_t + b$ , where  $W$  is the weight matrix and  $b$  is the bias term. We report normalized mean squared error (NMSE), defined as  $\mathbb{E}\|a_t - \hat{a}_t\|_2^2 / \text{Var}(a)$ . To standardize representation dimensionality across methods, we apply PCA to latent actions and keep  $d=128$  components, including the code length.

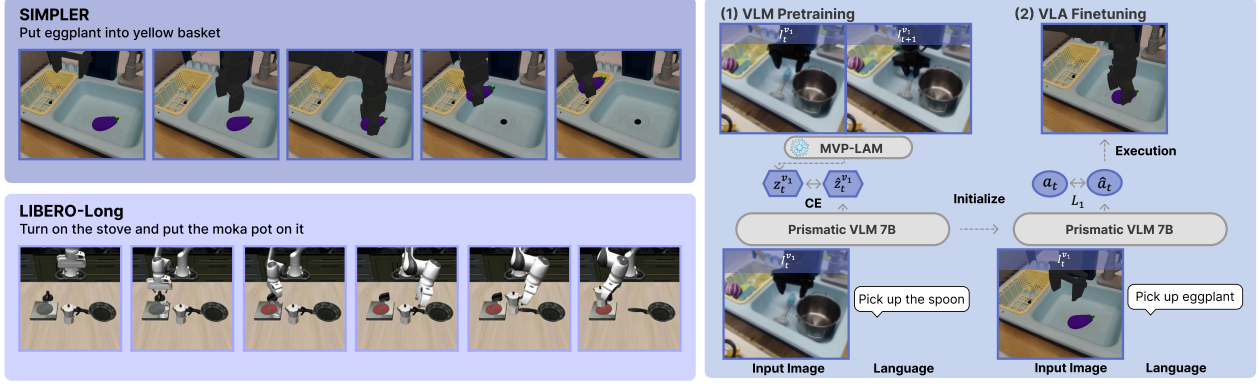


Figure 5. Overview of the VLM pretraining and VLA finetuning with example demonstrations. Left: sample observation sequences from SIMPLER and LIBERO-Long with natural language goal description. Right: (1) **VLM Pretraining**. Prismatic-7B VLM is pretrained to predict the discrete latent action token, which is produced by MVP-LAM, from an image and language instruction using a CE loss. (2) **VLA Finetuning**. VLA initializes from the pretrained VLM and finetunes on downstream demonstrations to predict robot actions.

**Results and analysis.** As shown in Figure 3, MVP-LAM achieves the highest estimated  $\mathcal{I}(Z; A)$  across all estimators, suggesting that its latent actions preserve more information about the actions than the baselines. Consistent with MI estimation, Figure 4 shows that MVP-LAM achieves lower NMSE on Bridge V2 and on OOD LIBERO suites (Spatial, Object, and Long), with a small drop on LIBERO-Goal relative to UniVLA. Overall, MI estimation and probing consistently indicate that MVP-LAM learns more action-centric latent actions. We note that UniVLA may struggle to achieve action-centricity because its training objective is primarily driven by task information from language descriptions, which are typically trajectory-level, and this provides weaker supervision for encoding step-level action signals in  $z_t$ . The details of linear probing and extended analysis including LAPA and Moto are listed in Appendix B.

### 4.3. Is MVP-LAM Effective for Manipulation?

**Benchmarks.** To examine whether VLA pretrained with MVP-LAM benefits from its action-centricity, we evaluate downstream manipulation on SIMPLER and LIBERO-Long with a single image and natural language description. Figure 5 shows example demonstrations from both benchmarks.

SIMPLER has been shown to correlate with real-world performance even though it is simulation-based. We evaluate four SIMPLER tasks using a 7-DoF WidowX arm to assess generalization across diverse manipulation goals: StackG2Y (stack the green cube on the yellow block), Carrot2Plate (place the carrot on the plate), Spoon2Towel (place the spoon on the towel), and Eggplant2Bask (place the eggplant in the basket). Since SIMPLER does not provide an official finetuning dataset, we use 100 diverse trajectories collected by Ye et al. (2024) (25 per task) and report both grasp rate and success rate.

LIBERO-Long evaluates the long-horizon manipulation performance which is the most challenging subset of LIBERO suites. The evaluation consists of a suite of 10 long-horizon tasks with natural language goal descriptions. For each task, we evaluate 10 runs with 5 random seeds, and the results are reported as the average of success rate over all 10 tasks.

**Baselines.** We compare VLA pretrained by MVP-LAM latent actions against the following baselines. We provide the implementation details of the baselines in Appendix D.2.

- **Latent action baselines.** UniVLA (Bu et al., 2025) pretrained on Bridge V2 is our primary baseline since the only difference is the LAM used in VLA pretraining. In addition, we include LAPA (Ye et al., 2024) which is a representative latent action based VLA.
- **VLA baselines.** OpenVLA (Kim et al., 2024) is a VLA model that leverages a large-scale pretraining dataset, including OXE. Octo (Octo Model Team et al., 2023) is transformer-based policy baselines trained on diverse robotic datasets with a unified action representation. Finally, we include  $\pi_0$  (Black et al., 2026) which is state-of-the-art VLA model.

**VLA pretraining & finetuning.** Figure 5 shows the details of VLM pretraining and VLA finetuning. We pretrain a VLM to predict MVP-LAM latent actions using a CE objective. We start from a Prismatic-7B VLM checkpoint (Karamcheti et al., 2024) and pretrain on Bridge V2. We then convert the pretrained VLM into a VLA by finetuning with LoRA to predict the ground-truth robot action  $a_t$ . To predict continuous robot action from discrete VLM outputs, we follow the action prediction method of UniVLA based on multi-head attention. Implementation details for VLA pretraining and finetuning are provided in Appendix C.2.

Table 1. **SIMPLER** benchmark result. We report success rate and grasping rate (%) on the SIMPLER benchmark.  $\dagger$  denotes results reported in prior work. Best is **bolded** and second best is underlined.

Success Rate	MVP-LAM	UniVLA	LAPA $\dagger$	OpenVLA $\dagger$	Octo-Small	Octo-Base	$\pi_0$
StackG2Y	33.3	16.7	<b>54.2</b>	<u>41.6</u>	8.3	0.0	37.5
Carrot2Plate	<b>66.7</b>	20.8	45.8	<u>50.0</u>	33.3	37.5	33.3
Spoon2Towel	<u>66.7</u>	54.2	<b>70.8</b>	37.5	25.0	12.5	29.2
Eggplant2Bask	<b>75.0</b>	<u>66.7</u>	58.3	16.7	12.5	20.8	45.8
AVG	<b>60.4</b>	39.6	<u>57.3</u>	36.4	19.8	17.7	36.5
Grasping Rate							
StackG2Y	54.3	45.8	<u>62.5</u>	50.0	54.2	<b>70.8</b>	58.3
Carrot2Plate	<u>70.8</u>	37.5	58.3	66.6	<b>75.0</b>	54.2	58.3
Spoon2Towel	<u>79.2</u>	<u>79.2</u>	<b>83.3</b>	45.8	66.7	70.8	54.2
Eggplant2Bask	<u>95.8</u>	<b>100.0</b>	83.3	37.5	50.0	54.2	87.5
AVG	<b>75.0</b>	65.6	<u>71.9</u>	50.0	61.5	62.5	64.6

**Results and analysis.** Table 1 shows that pretraining with MVP-LAM’s latent actions improves downstream manipulation over other baselines. In particular, MVP-LAM increases the average success rate from 39.6% (UniVLA) to 60.4%, with gains on all four tasks. While LAPA achieves strong performance on some tasks, MVP-LAM remains competitive overall and yields the best average success rate.

Table 2 reports results on LIBERO-Long. MVP-LAM achieves 90.8% success, improving over UniVLA pretrained on Bridge V2 (79.4%). It also outperforms OpenVLA and  $\pi_0$ , and is comparable to UniVLA pretrained on OXE-scale.

Table 2. **LIBERO-Long** results. Success rate (%) on LIBERO-Long.  $\dagger$  indicates results reported in prior work and  $*$  indicates the methods that use additional wrist-view images and states. UniVLA (Bridge) uses a Bridge V2-pretrained VLM, while UniVLA (OXE) uses an OXE-pretrained VLM. Best is **bolded** and second best is underlined.

MVP-LAM	UniVLA (Bridge)	OpenVLA $\dagger$	$\pi_0$ $\dagger*$	UniVLA $\dagger$ (OXE)
<b>90.8</b>	<u>79.4</u>	53.7	85.2	92.0

Despite using a substantially smaller robot dataset for VLM pretraining ( $\leq 60k$  trajectories) than OXE-scale pretraining (typically  $\geq 970k$  trajectories), MVP-LAM remains competitive on both SIMPLER and LIBERO-Long benchmarks. Notably, LIBERO-Long is used neither for VLM pretraining nor for LAM training, yet MVP-LAM attains a higher success rate. This improvement is consistent with the higher action-centricity of MVP-LAM latent actions (measured on Bridge V2 and LIBERO-Long). These results suggest that more action-centric latent actions provide a stronger pretraining signal and can translate into improved VLA finetuning performance.

#### 4.4. Does MVP-LAM Preserve Transition Information Under Viewpoint Perturbation?

We evaluate whether LAMs preserve transition-relevant information under viewpoint perturbations. On Bridge V2, we construct 3.7k viewpoint-perturbed transitions using a NVS model. For original Bridge trajectory  $\{I_t, a_t\}_{t=1}^T$ , we construct viewpoint-perturbed trajectory  $\{\tilde{I}_t, a_t\}_{t=1}^T$  by synthesizing each image  $I_t$  into  $\tilde{I}_t$ . Figure 6 shows an example of an original trajectory and its viewpoint-perturbed counterpart.

**Evaluation setup.** Measuring  $\mathcal{I}(Z_t; V_t, V_{t+1} \mid S_t, S_{t+1})$  requires viewpoint labels, which are not available in Bridge V2. We therefore use prediction error as an empirical proxy for how much viewpoint-dependent information remains in the latent action beyond the underlying state transition. We denote  $o_t = f(I_t)$  and  $\tilde{o}_t = f(\tilde{I}_t)$ . Then, we extract latent actions from the original transition  $(o_t, o_{t+1})$  and perturbed one  $(o_t, \tilde{o}_{t+1})$ , denoting them by  $z_t$  and  $\tilde{z}_t$ , respectively. To standardize evaluation, we measure prediction errors in the DINOv2 feature space. We denote DINOv2 by  $f_{\text{dino}}(\cdot)$ , define  $o_{t+1}^{\text{dino}} = f_{\text{dino}}(I_{t+1})$ , and let  $\hat{o}_{t+1}^{\text{dino}}(z)$  be the predicted next observation in the DINOv2 space from  $z_t$ . For LAMs that predict pixels, we embed decoded frames with  $f_{\text{dino}}$ .

$$\text{MSE} = \|o_{t+1}^{\text{dino}} - \hat{o}_{t+1}^{\text{dino}}(z_t)\|_2^2, \widetilde{\text{MSE}} = \|o_{t+1}^{\text{dino}} - \hat{o}_{t+1}^{\text{dino}}(\tilde{z}_t)\|_2^2.$$

Concretely,  $\text{MSE}$  uses  $z_t$  from the original transition, whereas  $\widetilde{\text{MSE}}$  uses  $\tilde{z}_t$  from the viewpoint-perturbed transition. Since  $I_{t+1}$  and  $\tilde{I}_{t+1}$  capture the same underlying state under different viewpoints, a larger  $\widetilde{\text{MSE}}$  suggests that the latent action is not purely determined by the state transition, but also depends on the viewpoint variation. This corresponds to  $Z_t$  retaining more viewpoint-dependent factors beyond  $(S_t, S_{t+1})$ , which aligns with a larger  $\mathcal{I}(Z_t; V_t, V_{t+1} \mid S_t, S_{t+1})$ .

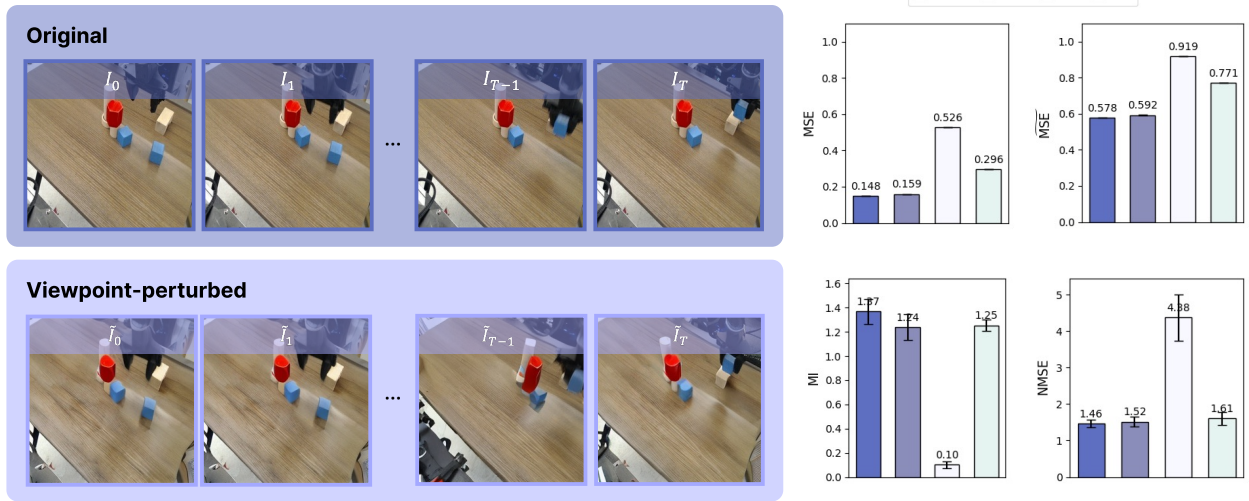


**Figure 6. Viewpoint perturbed trajectory and evaluation.** (Left): an example trajectory from the original camera view  $\{I_t\}$  (top) and its viewpoint perturbed counterpart  $\{\tilde{I}_t\}$  (bottom). (Right): reconstruction error on the original and perturbed sequences (top), reporting MSE and MRE and action-centricity metrics (bottom), reporting KSG mutual information and NMSE of linear probing, for MVP-LAM and baselines. Error bars show standard deviation over 3 random seeds.

Beyond observation level reconstruction errors, we analyze the action-centricity of latent actions under the viewpoint variations. We report (i) the estimated mutual information  $\hat{I}(\hat{Z}; A)$  computed from perturbed latent action  $\hat{Z}$ , and (ii) NMSE for a linear probe trained on latent action from the original view and evaluated on latent actions from perturbed views. For MI estimation, we use KSG with same evaluation protocol in Section 4.2, and do so for linear probing.

**Results and analysis.** As shown in Figure 6, MVP-LAM attains the lowest MSE on the original sequences, which indicates accurate next observation prediction on unperturbed transitions. It also achieves the lowest MRE, which suggests that prediction accuracy is largely preserved even when the latent action is inferred from a viewpoint perturbed transition. In addition, MVP-LAM preserves the action centricity signals, with the highest KSG mutual information and the lowest cross view probing error, outperforming all baselines.

These results support the claim that MVP-LAM preserves transition relevant information under viewpoint perturbations. While the metrics in Figure 6 are empirical proxies and do not directly estimate  $I(Z_t; V_t, V_{t+1} | S_t, S_{t+1})$ , MVP-LAM consistently outperforms the baselines on MRE and action-centricity, which is aligned with a reduction of viewpoint dependent information in the inferred latent action. We further provide qualitative and quantitative results for pixel based LAMs, which degrade substantially when conditioning the decoder on latent actions inferred from perturbed transitions, in Appendix E.3.

#### 4.5. Ablation Study

We study which components of MVP-LAM are responsible for action-centric latent actions. We ablate (i) the human video dataset in the MVP-LAM training mixture and (ii) the cross-viewpoint reconstruction term in  $\mathcal{L}_{\text{MVP-LAM}}$ . All ablations use the same LAM architecture and training hyperparameters, and follow the same evaluation protocol as Section 4.2.

**Is the human dataset beneficial to MVP-LAM?** Table 3 shows improved action-centricity on Bridge V2 when human videos are included in MVP-LAM training. In particular, the model trained with human videos outperforms the robot-only baseline on both MI and NMSE. This suggests that including human videos during MVP-LAM training can improve action-centricity. We hypothesize that training MVP-LAM solely on robot data leads to overfitting due to limited motion and scene diversity. The diversity of motion and backgrounds in robot dataset is highly limited as it is collected in relatively controlled settings. Since LAMs tend to encode factors that explain large frame-to-frame variation in the transitions (Zhang et al., 2025), such limited diversity can increase the risk that the LAM encodes incidental variations in addition to the agent’s motion. Meanwhile, human videos provide substantially higher diversity in both motions and scenes, which makes such incidental variations less predictive and encourages the model to prioritize motion as the dominant source of transition, leading to more action-centric latent actions.

**Table 3. Ablations over training data and  $\mathcal{L}_{\text{cross}}$ .** Robot and Human indicate whether robot or human multi-view videos are included in LAM training, and  $\mathcal{L}_{\text{cross}}$  indicates whether cross-viewpoint reconstruction is enabled. We report NMSE of linear probe and estimated MI (KSG), with mean $\pm$ std over 4 seeds.

Robot	Human	$\mathcal{L}_{\text{cross}}$	NMSE $\downarrow$	MI (KSG) $\uparrow$
✓		✓	$0.91 \pm 0.01$	$0.50 \pm 0.03$
✓	✓		$0.96 \pm 0.01$	$0.27 \pm 0.01$
✓	✓	✓	<b><math>0.73 \pm 0.01</math></b>	<b><math>1.10 \pm 0.03</math></b>

**How does cross-viewpoint reconstruction affect MVP-LAM?** Table 3 shows that removing  $\mathcal{L}_{\text{cross}}$  reduces action-centricity, as reflected by lower MI with ground-truth actions and lower action prediction accuracy of MVP-LAM without cross-viewpoint reconstruction. This suggests that training on multi-view videos with self-viewpoint reconstruction alone is insufficient to learn action-centric latent actions. The observed action-centricity of MVP-LAM is therefore primarily associated with the cross-viewpoint reconstruction objective, rather than multi-view training alone.

## 5. Conclusion and Limitations

**Limitations and future works.** Our approach relies on time-synchronized multi-view videos during LAM training. While multi-view capture can be more feasible for human videos than collecting large-scale robot demonstrations, it still requires additional instrumentation and synchronization compared to single-view human data. In addition, while SIMPLER has been shown to correlate with real-world performance, our evaluation is limited to simulation benchmarks and does not include real-world robot experiments. A promising direction for future work is to train MVP-LAM on weakly synchronized or pseudo-paired multi-view videos, thereby relaxing the strict synchronization requirement. Finally, while this work focuses on viewpoint variation as an exogenous noise, identifying and mitigating other noise such as background motion remains important future work.

**Conclusion.** In summary, we propose MVP-LAM, a latent action model that learns discrete latent actions from time-synchronized multi-view videos using a cross-viewpoint reconstruction objective. We show that cross-viewpoint reconstruction improves action-centricity on Bridge V2, as measured by higher estimated mutual information and lower linear probe NMSE to ground-truth robot actions. We further show that using MVP-LAM latent actions as pseudo-labels for VLA pretraining improves downstream manipulation on SIMPLER and LIBERO-Long. Finally, we show that MVP-LAM preserves transition-relevant information under viewpoint variation on Bridge V2 using novel view synthesized samples.

## References

Agibot-World-Contributors, Bu, Q., Cai, J., Chen, L., Cui, X., Ding, Y., Feng, S., Gao, S., He, X., Hu, X., Huang, X., Jiang, S., Jiang, Y., Jing, C., Li, H., Li, J., Liu, C., Liu, Y., Lu, Y., Luo, J., Luo, P., Mu, Y., Niu, Y., Pan, Y., Pang, J., Qiao, Y., Ren, G., Ruan, C., Shan, J., Shen, Y., Shi, C., Shi, M., Shi, M., Sima, C., Song, J., Wang, H., Wang, W., Wei, D., Xie, C., Xu, G., Yan, J., Yang, C., Yang, L., Yang, S., Yao, M., Zeng, J., Zhang, C., Zhang, Q., Zhao, B., Zhao, C., Zhao, J., and Zhu, J. Agibot world colosse: A large-scale manipulation platform for scalable and intelligent embodied systems, 2025. URL <https://arxiv.org/abs/2503.06669>.

Alain, G. and Bengio, Y. Understanding intermediate layers using linear classifier probes, 2017. URL <https://openreview.net/forum?id=ryF7rTqgl>.

Bahl, S., Mendonca, R., Chen, L., Jain, U., and Pathak, D. Affordances from human videos as a versatile representation for robotics. 2023.

Barber, D. and Agakov, F. V. The im algorithm: a variational approach to information maximization. In *Neural Information Processing Systems*, 2003. URL <https://api.semanticscholar.org/CorpusID:14633080>.

Belghazi, M. I., Baratin, A., Rajeshwar, S., Ozair, S., Bengio, Y., Courville, A., and Hjelm, D. Mutual information neural estimation. In Dy, J. and Krause, A. (eds.), *Proceedings of the 35th International Conference on Machine Learning*, volume 80 of *Proceedings of Machine Learning Research*, pp. 531–540. PMLR, 10–15 Jul 2018. URL <https://proceedings.mlr.press/v80/belghazi18a.html>.

Bharadhwaj, H., Gupta, A., Kumar, V., and Tulsiani, S. Towards generalizable zero-shot manipulation via translating human interaction plans, 2023.

Bharadhwaj, H., Mottaghi, R., Gupta, A., and Tulsiani, S. Track2act: Predicting point tracks from internet videos enables generalizable robot manipulation. In *European Conference on Computer Vision (ECCV)*, 2024.

Black, K., Brown, N., Driess, D., Esmail, A., Equi, M., Finn, C., Fusai, N., Groom, L., Hausman, K., Ichter, B., Jakubczak, S., Jones, T., Ke, L., Levine, S., Li-Bell, A., Mothukuri, M., Nair, S., Pertsch, K., Shi, L. X., Tanner, J., Vuong, Q., Walling, A., Wang, H., and Zhilinsky, U.  $\pi_0$ : A vision-language-action flow model for general robot control, 2026. URL <https://arxiv.org/abs/2410.24164>.

Bruce, J., Dennis, M., Edwards, A., Parker-Holder, J., Shi, Y., Hughes, E., Lai, M., Mavalankar, A., Steigerwald, R., Apps, C., Aytar, Y., Bechtle, S., Behbahani,

F., Chan, S., Heess, N., Gonzalez, L., Osindero, S., Ozair, S., Reed, S., Zhang, J., Zolna, K., Clune, J., de Freitas, N., Singh, S., and Rocktäschel, T. Geenie: Generative interactive environments, 2024. URL <https://arxiv.org/abs/2402.15391>.

Bu, Q., Yang, Y., Cai, J., Gao, S., Ren, G., Yao, M., Luo, P., and Li, H. Univla: Learning to act anywhere with task-centric latent actions. *arXiv preprint arXiv:2505.06111*, 2025.

Chen, L. Y., Xu, C., Dharmarajan, K., Irshad, M. Z., Cheng, R., Keutzer, K., Tomizuka, M., Vuong, Q., and Goldberg, K. Rovi-aug: Robot and viewpoint augmentation for cross-embodiment robot learning. In *Conference on Robot Learning (CoRL)*, Munich, Germany, 2024a.

Chen, X., Guo, J., He, T., Zhang, C., Zhang, P., Yang, D. C., Zhao, L., and Bian, J. IGOR: Image-GOal representations are the atomic building blocks for next-level generalization in embodied AI, 2025a. URL <https://openreview.net/forum?id=bpdzTIVq8>.

Chen, X., Wei, H., Zhang, P., Zhang, C., Wang, K., Guo, Y., Yang, R., Wang, Y., Xiao, X., Zhao, L., Chen, J., and Bian, J. villa-x: Enhancing latent action modeling in vision-language-action models. *arXiv preprint arXiv:2507.23682*, 2025b.

Chen, Y., Ge, Y., Li, Y., Ge, Y., Ding, M., Shan, Y., and Liu, X. Moto: Latent motion token as the bridging language for robot manipulation. *arXiv preprint arXiv:2412.04445*, 2024b.

Collaboration, O. X.-E., O'Neill, A., Rehman, A., Gupta, A., Maddukuri, A., Gupta, A., Padalkar, A., Lee, A., Pooley, A., Gupta, A., Mandlekar, A., Jain, A., Tung, A., Bewley, A., Herzog, A., Irpan, A., Khazatsky, A., Rai, A., Gupta, A., Wang, A., Kolobov, A., Singh, A., Garg, A., Kembhavi, A., Xie, A., Brohan, A., Raffin, A., Sharma, A., Yavary, A., Jain, A., Balakrishna, A., Wahid, A., Burgess-Limerick, B., Kim, B., Schölkopf, B., Wulfe, B., Ichter, B., Lu, C., Xu, C., Le, C., Finn, C., Wang, C., Xu, C., Chi, C., Huang, C., Chan, C., Agia, C., Pan, C., Fu, C., Devin, C., Xu, D., Morton, D., Driess, D., Chen, D., Pathak, D., Shah, D., Büchler, D., Jayaraman, D., Kalashnikov, D., Sadigh, D., Johns, E., Foster, E., Liu, F., Ceola, F., Xia, F., Zhao, F., Frujeri, F. V., Stulp, F., Zhou, G., Sukhatme, G. S., Salhotra, G., Yan, G., Feng, G., Schiavi, G., Berseth, G., Kahn, G., Yang, G., Wang, G., Su, H., Fang, H.-S., Shi, H., Bao, H., Amor, H. B., Christensen, H. I., Furuta, H., Bharadhwaj, H., Walke, H., Fang, H., Ha, H., Mordatch, I., Radosavovic, I., Leal, I., Liang, J., Abou-Chakra, J., Kim, J., Drake, J., Peters, J., Schneider, J., Hsu, J., Vakil, J., Bohg, J., Bingham, J., Wu, J., Gao, J., Hu, J., Wu, J., Wu, J., Sun, J., Luo, J., Gu, J., Tan, J., Oh, J., Wu, J., Lu, J., Yang, J., Malik, J., Silvério, J., Hejna, J., Booher, J., Tompson, J., Yang, J., Salvador, J., Lim, J. J., Han, J., Wang, K., Rao, K., Pertsch, K., Hausman, K., Go, K., Gopalakrishnan, K., Goldberg, K., Byrne, K., Oslund, K., Kawaharazuka, K., Black, K., Lin, K., Zhang, K., Ehsani, K., Lekkala, K., Ellis, K., Rana, K., Srinivasan, K., Fang, K., Singh, K. P., Zeng, K.-H., Hatch, K., Hsu, K., Itti, L., Chen, L. Y., Pinto, L., Fei-Fei, L., Tan, L., Fan, L. J., Ott, L., Lee, L., Weihs, L., Chen, M., Lepert, M., Memmel, M., Tomizuka, M., Itkina, M., Castro, M. G., Spero, M., Du, M., Ahn, M., Yip, M. C., Zhang, M., Ding, M., Heo, M., Srirama, M. K., Sharma, M., Kim, M. J., Irshad, M. Z., Kanazawa, N., Hansen, N., Heess, N., Joshi, N. J., Suenderhauf, N., Liu, N., Palo, N. D., Shafiuallah, N. M. M., Mees, O., Kroemer, O., Bastani, O., Sanketi, P. R., Miller, P. T., Yin, P., Wohlhart, P., Xu, P., Fagan, P. D., Mitrano, P., Sermanet, P., Abbeel, P., Sundaresan, P., Chen, Q., Vuong, Q., Rafailov, R., Tian, R., Doshi, R., Mart'in-Mart'in, R., Baijal, R., Scalise, R., Hendrix, R., Lin, R., Qian, R., Zhang, R., Mendonca, R., Shah, R., Hoque, R., Julian, R., Bustamante, S., Kirmani, S., Levine, S., Lin, S., Moore, S., Bahl, S., Dass, S., Sonawani, S., Tulsiani, S., Song, S., Xu, S., Haldar, S., Karamchetti, S., Adebola, S., Guist, S., Nasiriany, S., Schaal, S., Welker, S., Tian, S., Ramamoorthy, S., Dasari, S., Belkhale, S., Park, S., Nair, S., Mirchandani, S., Osa, T., Gupta, T., Harada, T., Matsushima, T., Xiao, T., Kollar, T., Yu, T., Ding, T., Davchev, T., Zhao, T. Z., Armstrong, T., Darrell, T., Chung, T., Jain, V., Kumar, V., Vanhoucke, V., Guizilini, V., Zhan, W., Zhou, W., Burgard, W., Chen, X., Chen, X., Wang, X., Zhu, X., Geng, X., Liu, X., Liangwei, X., Li, X., Pang, Y., Lu, Y., Ma, Y. J., Kim, Y., Chebotar, Y., Zhou, Y., Zhu, Y., Wu, Y., Xu, Y., Wang, Y., Bisk, Y., Dou, Y., Cho, Y., Lee, Y., Cui, Y., Cao, Y., Wu, Y.-H., Tang, Y., Zhu, Y., Zhang, Y., Jiang, Y., Li, Y., Li, Y., Iwasawa, Y., Matsuo, Y., Ma, Z., Xu, Z., Cui, Z. J., Zhang, Z., Fu, Z., and Lin, Z. Open X-Embodiment: Robotic learning datasets and RT-X models. <https://arxiv.org/abs/2310.08864>, 2023.

Driess, D., Schubert, I., Florence, P., Li, Y., and Toussaint, M. Reinforcement learning with neural radiance fields. In *Advances in Neural Information Processing Systems (NeurIPS)*, 2022.

Goyal, A., Xu, J., Guo, Y., Blukis, V., Chao, Y.-W., and Fox, D. Rvt: Robotic view transformer for 3d object manipulation. *arXiv:2306.14896*, 2023.

Grauman, K., Westbury, A., Torresani, L., Kitani, K., Malik, J., Afouras, T., Ashutosh, K., Baiyya, V., Bansal, S., Boote, B., Byrne, E., Chavis, Z., Chen, J., Cheng, F., Chu, F.-J., Crane, S., Dasgupta, A., Dong, J., Escobar, M., Forigua, C., Gebreselasie, A., Haresh, S., Huang,

J., Islam, M. M., Jain, S., Khirodkar, R., Kukreja, D., Liang, K. J., Liu, J.-W., Majumder, S., Mao, Y., Martin, M., Mavroudi, E., Nagarajan, T., Ragusa, F., Ramakrishnan, S. K., Seminara, L., Somayazulu, A., Song, Y., Su, S., Xue, Z., Zhang, E., Zhang, J., Castillo, A., Chen, C., Fu, X., Furuta, R., Gonzalez, C., Gupta, P., Hu, J., Huang, Y., Huang, Y., Khoo, W., Kumar, A., Kuo, R., Lakhavani, S., Liu, M., Luo, M., Luo, Z., Meredith, B., Miller, A., Oguntola, O., Pan, X., Peng, P., Pramanick, S., Ramazanova, M., Ryan, F., Shan, W., Somasundaram, K., Song, C., Southerland, A., Tateno, M., Wang, H., Wang, Y., Yagi, T., Yan, M., Yang, X., Yu, Z., Zha, S. C., Zhao, C., Zhao, Z., Zhu, Z., Zhuo, J., Arbelaez, P., Bertasius, G., Damen, D., Engel, J., Farinella, G. M., Furnari, A., Ghanem, B., Hoffman, J., Jawahar, C., Newcombe, R., Park, H. S., Rehg, J. M., Sato, Y., Savva, M., Shi, J., Shou, M. Z., and Wray, M. Ego-exo4d: Understanding skilled human activity from first- and third-person perspectives. In *Proceedings of the IEEE/CVF Conference on Computer Vision and Pattern Recognition (CVPR)*, pp. 19383–19400, June 2024.

Ha, D. and Schmidhuber, J. World models. 2018. doi: 10.5281/ZENODO.1207631. URL <https://zenodo.org/record/1207631>.

He, K., Chen, X., Xie, S., Li, Y., Dollár, P., and Girshick, R. Masked autoencoders are scalable vision learners. In *2022 IEEE/CVF Conference on Computer Vision and Pattern Recognition (CVPR)*, pp. 15979–15988, 2022. doi: 10.1109/CVPR52688.2022.01553.

Hirose, N., Shah, D., Sridhar, A., and Levine, S. Exaug: Robot-conditioned navigation policies via geometric experience augmentation. *arXiv preprint arXiv:2210.07450*, 2022.

Karamcheti, S., Nair, S., Balakrishna, A., Liang, P., Kollar, T., and Sadigh, D. Prismatic vlms: Investigating the design space of visually-conditioned language models. In *International Conference on Machine Learning (ICML)*, 2024.

Khazatsky, A., Pertsch, K., Nair, S., Balakrishna, A., Dasari, S., Karamcheti, S., Nasiriany, S., Srirama, M. K., Chen, L. Y., Ellis, K., Fagan, P. D., Hejna, J., Itkina, M., Lepert, M., Ma, Y. J., Miller, P. T., Wu, J., Belkhale, S., Dass, S., Ha, H., Jain, A., Lee, A., Lee, Y., Memmel, M., Park, S., Radosavovic, I., Wang, K., Zhan, A., Black, K., Chi, C., Hatch, K. B., Lin, S., Lu, J., Mercat, J., Rehman, A., Sanketi, P. R., Sharma, A., Simpson, C., Vuong, Q., Walke, H. R., Wulfe, B., Xiao, T., Yang, J. H., Yavary, A., Zhao, T. Z., Agia, C., Baijal, R., Castro, M. G., Chen, D., Chen, Q., Chung, T., Drake, J., Foster, E. P., Gao, J., Guizilini, V., Herrera, D. A., Heo, M., Hsu, K., Hu, J., Irshad, M. Z., Jackson, D., Le, C., Li, Y., Lin, K., Lin, R., Ma, Z., Maddukuri, A., Mirchandani, S., Morton, D., Nguyen, T., O'Neill, A., Scalise, R., Seale, D., Son, V., Tian, S., Tran, E., Wang, A. E., Wu, Y., Xie, A., Yang, J., Yin, P., Zhang, Y., Bastani, O., Berseth, G., Bohg, J., Goldberg, K., Gupta, A., Gupta, A., Jayaraman, D., Lim, J. J., Malik, J., Martín-Martín, R., Ramamoorthy, S., Sadigh, D., Song, S., Wu, J., Yip, M. C., Zhu, Y., Kollar, T., Levine, S., and Finn, C. Droid: A large-scale in-the-wild robot manipulation dataset. 2024.

Kim, H., Kang, J., Kang, H., Cho, M., Kim, S. J., and Lee, Y. Uniskill: Imitating human videos via cross-embodiment skill representations. *arXiv preprint arXiv:2505.08787*, 2025a.

Kim, M., Pertsch, K., Karamcheti, S., Xiao, T., Balakrishna, A., Nair, S., Rafailov, R., Foster, E., Lam, G., Sanketi, P., Vuong, Q., Kollar, T., Burchfiel, B., Tedrake, R., Sadigh, D., Levine, S., Liang, P., and Finn, C. Openvla: An open-source vision-language-action model. *arXiv preprint arXiv:2406.09246*, 2024.

Kim, M. J., Finn, C., and Liang, P. Fine-tuning vision-language-action models: Optimizing speed and success. *arXiv preprint arXiv:2502.19645*, 2025b.

Klepach, A., Nikulin, A., Zisman, I., Tarasov, D., Derevyagin, A., Polubarov, A., Nikita, L., and Kurenkov, V. Object-centric latent action learning. In *7th Robot Learning Workshop: Towards Robots with Human-Level Abilities*, 2025. URL <https://openreview.net/forum?id=JStiQojug>.

Kwon, T., Tekin, B., Stühmer, J., Bogo, F., and Pollefeys, M. H2o: Two hands manipulating objects for first person interaction recognition. In *Proceedings of the IEEE/CVF International Conference on Computer Vision (ICCV)*, pp. 10138–10148, October 2021.

Li, X., Hsu, K., Gu, J., Pertsch, K., Mees, O., Walke, H. R., Fu, C., Lunawat, I., Sieh, I., Kirmani, S., Levine, S., Wu, J., Finn, C., Su, H., Vuong, Q., and Xiao, T. Evaluating real-world robot manipulation policies in simulation. *arXiv preprint arXiv:2405.05941*, 2024.

Liu, B., Zhu, Y., Gao, C., Feng, Y., Liu, Q., Zhu, Y., and Stone, P. Libero: Benchmarking knowledge transfer for lifelong robot learning. *arXiv preprint arXiv:2306.03310*, 2023.

McCarthy, R., Tan, D. C. H., Schmidt, D., Acero, F., Herr, N., Du, Y., Thuruthel, T. G., and Li, Z. Towards generalist robot learning from internet video: A survey, 2024. URL <https://arxiv.org/abs/2404.19664>.

Misra, D., Saran, A., Xie, T., Lamb, A., and Langford, J. Towards principled representation learning from

videos for reinforcement learning. In *The Twelfth International Conference on Learning Representations*, 2024. URL <https://openreview.net/forum?id=3mnWvUZIXt>.

Nair, S., Rajeswaran, A., Kumar, V., Finn, C., and Gupta, A. R3m: A universal visual representation for robot manipulation, 2022. URL <https://arxiv.org/abs/2203.12601>.

Nikulin, A., Zisman, I., Klepach, A., Tarasov, D., Derevyagin, A., Polubarov, A., Nikita, L., and Kurenkov, V. Vision-language models unlock task-centric latent actions. In *Workshop on Scaling Environments for Agents*, 2025a. URL <https://openreview.net/forum?id=FgRLKZRfk3>.

Nikulin, A., Zisman, I., Tarasov, D., Nikita, L., Polubarov, A., Kiselev, I., and Kurenkov, V. Latent action learning requires supervision in the presence of distractors. In *Forty-second International Conference on Machine Learning*, 2025b. URL <https://openreview.net/forum?id=2gcEQCT7QW>.

Octo Model Team, Ghosh, D., Walke, H., Pertsch, K., Black, K., Mees, O., Dasari, S., Hejna, J., Xu, C., Luo, J., Kreiman, T., Tan, Y., Sadigh, D., Finn, C., and Levine, S. Octo: An open-source generalist robot policy, 2023.

Quab, M., Darcet, T., Moutakanni, T., Vo, H. V., Szafraniec, M., Khalidov, V., Fernandez, P., HAZIZA, D., Massa, F., El-Nouby, A., Assran, M., Ballas, N., Galuba, W., Howes, R., Huang, P.-Y., Li, S.-W., Misra, I., Rabbat, M., Sharma, V., Synnaeve, G., Xu, H., Jegou, H., Mairal, J., Labatut, P., Joulin, A., and Bojanowski, P. DINOv2: Learning robust visual features without supervision. *Transactions on Machine Learning Research*, 2024. ISSN 2835-8856. URL <https://openreview.net/forum?id=a68SUt6zFt>. Featured Certification.

Schmidt, D. and Jiang, M. Learning to act without actions. In *The Twelfth International Conference on Learning Representations (ICLR)*, 2024.

Sener, F., Chatterjee, D., Sheleporov, D., He, K., Singhania, D., Wang, R., and Yao, A. Assembly101: A large-scale multi-view video dataset for understanding procedural activities. *CVPR 2022*.

Sermanet, P., Lynch, C., Chebotar, Y., Hsu, J., Jang, E., Schaal, S., Levine, S., and Brain, G. Time-contrastive networks: Self-supervised learning from video. In *2018 IEEE International Conference on Robotics and Automation (ICRA)*, pp. 1134–1141, 2018. doi: 10.1109/ICRA.2018.8462891.

Shim, D., Lee, S., and Kim, H. J. Snerl: Semantic-aware neural radiance fields for reinforcement learning. In *International Conference on Machine Learning*. PMLR, 2023.

Srirama, M. K., Dasari, S., Bahl, S., and Gupta, A. Hrp: Human affordances for robotic pre-training. In *Proceedings of Robotics: Science and Systems*, Delft, Netherlands, 2024.

Tian, S., Wulfe, B., Sargent, K., Liu, K., Zakharov, S., Guizilini, V., and Wu, J. View-invariant policy learning via zero-shot novel view synthesis. *arXiv*, 2024.

van den Oord, A., Vinyals, O., and Kavukcuoglu, K. Neural discrete representation learning. In *Proceedings of the 31st International Conference on Neural Information Processing Systems*, NIPS’17, pp. 6309–6318, Red Hook, NY, USA, 2017. Curran Associates Inc. ISBN 9781510860964.

Walke, H., Black, K., Lee, A., Kim, M. J., Du, M., Zheng, C., Zhao, T., Hansen-Estruch, P., Vuong, Q., He, A., Myers, V., Fang, K., Finn, C., and Levine, S. Bridgedata v2: A dataset for robot learning at scale. In *Conference on Robot Learning (CoRL)*, 2023.

Wang, Y., Zhang, F., Zhan, D.-C., Zhao, L., Wang, K., and Bian, J. Co-evolving latent action world models, 2025. URL <https://arxiv.org/abs/2510.26433>.

Wen, C., Lin, X., So, J., Chen, K., Dou, Q., Gao, Y., and Abbeel, P. Any-point trajectory modeling for policy learning, 2023.

Ye, S., Jang, J., Jeon, B., Joo, S., Yang, J., Peng, B., Mandlekar, A., Tan, R., Chao, Y.-W., Lin, B. Y., Liden, L., Lee, K., Gao, J., Zettlemoyer, L., Fox, D., and Seo, M. Latent action pretraining from videos, 2024. URL <https://arxiv.org/abs/2410.11758>.

Ze, Y., Zhang, G., Zhang, K., Hu, C., Wang, M., and Xu, H. 3d diffusion policy: Generalizable visuomotor policy learning via simple 3d representations. In *Proceedings of Robotics: Science and Systems (RSS)*, 2024.

Zhang, C., Pearce, T., Zhang, P., Wang, K., Chen, X., Shen, W., Zhao, L., and Bian, J. What do latent action models actually learn? In *The Thirty-ninth Annual Conference on Neural Information Processing Systems*, 2025. URL <https://openreview.net/forum?id=DQMjemrVhe>.

Zheng, H., Lee, R., and Lu, Y. Ha-vid: A human assembly video dataset for comprehensive assembly knowledge understanding. In Oh, A., Naumann, T., Globerson, A., Saenko, K., Hardt, M., and Levine, S. (eds.), *Advances in Neural Information Processing Systems*,

volume 36, pp. 67069–67081. Curran Associates, Inc., 2023. URL [https://proceedings.neurips.cc/paper\\_files/paper/2023/file/d40e6e4b3ee6c24f2bf2cb72c2412f4b-Paper-Datasets\\_and\\_Benchmarks.pdf](https://proceedings.neurips.cc/paper_files/paper/2023/file/d40e6e4b3ee6c24f2bf2cb72c2412f4b-Paper-Datasets_and_Benchmarks.pdf).

Zhu, Y., Jiang, Z., Stone, P., and Zhu, Y. Learning generalizable manipulation policies with object-centric 3d representations. In *7th Annual Conference on Robot Learning*, 2023.

## A. Relation of Action-centric Latent Action and Viewpoints

We provide the theoretical motivation of reducing the effect of viewpoint variation for action-centric latent actions. For brevity, we drop the time index and write  $(S, S') = (S_t, S_{t+1})$  and  $(V, V') = (V_t, V_{t+1})$  (similarly for  $(O, O')$ ). We assume the observation  $O$  is a deterministic function of  $S, V$ , i.e.  $O = g(S, V)$ . We neglect the noise in pixel-level (e.g., lighting variation and sensor noise) since  $O$  is often in feature space of the vision encoder. Then,

$$\begin{aligned}\mathcal{I}(Z; A) &= \mathcal{I}(Z; S, A, S') - \mathcal{I}(Z; S, S'|A) \\ &\geq \mathcal{I}(Z; S, S') - \mathcal{H}(S, S'|A)\end{aligned}$$

where  $\mathcal{I}(\cdot; \cdot)$  is mutual information and  $\mathcal{H}(\cdot)$  is entropy. By the chain rule,

$$\mathcal{I}(Z; S, S') = \mathcal{I}(Z; S, V, S', V') - \mathcal{I}(Z; V, V' | S, S'),$$

which implies

$$\mathcal{I}(Z; A) \geq \mathcal{I}(Z; S, V, S', V') - \mathcal{I}(Z; V, V' | S, S') - \mathcal{H}(S, S' | A). \quad (9)$$

Now consider a fixed-capacity discrete bottleneck (e.g., VQ-VAE with codebook size  $K$ ), where  $\mathcal{I}(Z; O, O') \leq \mathcal{H}(Z) \leq \log K$ . Since we use deterministic encoder  $E$  and assume  $O = g(S, V)$ ,

$$0 = \mathcal{H}(Z|O, O') = \mathcal{H}(Z|S, V, S', V') \quad (10)$$

Therefore,

$$\mathcal{I}(Z; S, V, S', V') = \mathcal{H}(Z) \leq \log K \quad (11)$$

Then (9) implies

$$\mathcal{I}(Z; A) \geq \mathcal{H}(Z) - \mathcal{I}(Z; V, V' | S, S') - \mathcal{H}(S, S' | A). \quad (12)$$

Since  $\mathcal{H}(S, S' | A)$  is constant under our assumptions, the only representation-dependent term in the bound is  $\mathcal{H}(Z)$  and  $\mathcal{I}(Z; V, V' | S, S')$ . Therefore, minimizing  $\mathcal{I}(Z; V, V' | S, S')$  is beneficial as long as it does not cause representation collapse, i.e., does not substantially reduce  $\mathcal{H}(Z)$  under the fixed-capacity constraint.

## B. Action-centricity Estimation Details

**Action normalization.** Robot actions are often provided in a per-timestep normalized space, where each 7D action  $a_t$  is z-scored using dataset-level statistics. In our evaluation, we convert such sequences into a *net relative action* representation that aggregates a multi-step action sequence into a single 7D vector while keeping the scale comparable across different horizons.

Specifically, when the actions are stored as  $a^{\text{norm}} \in \mathbb{R}^{B \times H \times 7}$ , we first recover actions in the original scale via per-dimension de-normalization,

$$a_t^{\text{raw}} = a_t^{\text{norm}} \odot \sigma + \mu, \quad (13)$$

where  $(\mu, \sigma)$  are dataset-specific mean and standard deviation and  $\odot$  denotes elementwise multiplication. We then form a net action  $a^{\text{net}} \in \mathbb{R}^{B \times 7}$  by summing the first six continuous control dimensions over time and taking the final gripper command as the seventh dimension:

$$a_{1:6}^{\text{net}} = \sum_{t=1}^H a_{t,1:6}^{\text{raw}}, \quad a_7^{\text{net}} = a_{H,7}^{\text{raw}}. \quad (14)$$

Finally, we re-normalize the net action with horizon-aware statistics so that the net action remains in a standardized space:

$$\hat{\mu}_{1:6} = H\mu_{1:6}, \quad \hat{\sigma}_{1:6} = \sqrt{H}\sigma_{1:6}, \quad \hat{\mu}_7 = \mu_7, \quad \hat{\sigma}_7 = \sigma_7, \quad (15)$$

$$a^{\text{net-norm}} = (a^{\text{net}} - \hat{\mu}) \oslash (\hat{\sigma} + \epsilon), \quad (16)$$

where  $\oslash$  is elementwise division and  $\epsilon$  is a small constant for numerical stability. We use such normalization protocol in both mutual information estimation and linear probing. This aggregation yields a horizon-consistent 7D target: unlike flattening a  $H$ -step sequence into a  $7H$ -dimensional label, it keeps the dimension of neural networks fixed across horizons, enabling fair comparisons without changing the capacity. Unlike averaging, summation preserves the semantics of cumulative control and avoids introducing a horizon-dependent rescaling of the target.

Table 4. Hyperparameters for MI estimation and linear probing. Hyperparameters related to training (upper) and the model (lower) in neural MI estimation and linear probing.

Hyperparameters	MI estimation	Linear probing
Batch Size	1024	512
Epochs/Steps	8000 steps	30 epochs
Learning Rate	1e-4/5e-5 (MINE/BA)	1e-3
Scheduler	–	Cosine
Gradient Clip	1.0	0.0
Weight Decay	1e-5	0.0
Hidden Dim.	1024	64
Depth	4	1

## B.1. Mutual Information

We evaluate how much information the latent action representation  $z_t$  retains about the ground-truth action  $a$  on the Bridge V2 dataset. Given an observation pair  $(o_t^{(i)}, o_{t+1}^{(i)})$ , we compute a latent action  $z_t^{(i)} = \text{Quantize}(E(o_t^{(i)}, o_{t+1}^{(i)}))$ . We estimate the mutual information  $\mathcal{I}(Z; A)$  using three complementary estimators: a non-parametric kNN estimator (KSG) and a neural variational estimator (BA, MINE). As a sanity check, we additionally compute a mismatch score by randomly permuting the pairing between  $\{z_t^{(i)}\}$  and  $\{a_t^{(i)}\}$  at test time, which significantly decreases the estimated dependence. When training the neural MI estimators, we freeze the LAM and optimize only the estimator network.

**KSG (kNN-based MI).** We apply the Kraskov–Stögbauer–Grassberger (KSG) estimator on the paired samples  $\{(z_t^{(i)}, a_t^{(i)})\}_{i=1}^N$ . Before estimation, we standardize each dimension of  $z$  and  $a$  using z-score normalization computed on the evaluation split. Since KSG is unstable in high dimensions, we apply a random projection with  $W \sim \mathcal{N}(\mathbf{0}, \mathbf{I})$  to each latent action  $z_t^{(i)} \in \mathbb{R}^d$ .

$$\tilde{z}_t^{(i)} = W z_t^{(i)} \in \mathbb{R}^{256} \quad (17)$$

Since random projection discards information, the estimated mutual information after projection is a lower bound on the true mutual information in the original latent space. We use  $k = 5$  for every evaluation.

**MINE (DV variational lower bound).** We train a critic  $T_\theta(z, a)$  using the Donsker–Varadhan (DV) representation:

$$\mathcal{I}(Z; A) \geq \mathbb{E}_{p(z, a)}[T_\theta(z, a)] - \log \mathbb{E}_{p(z)p(a)}[\exp(T_\theta(z, a))]. \quad (18)$$

In practice, we approximate samples from  $p(z)p(a)$  by shuffling actions within each minibatch (in-batch product-of-marginals). We report the bound on the held-out test split (in bits), and to reduce variance from shuffling, we average the second term over multiple independent shuffles per minibatch.

**Barber–Agakov (BA) variational estimator.** To complement kNN-based and critic-based estimators, we additionally estimate  $\mathcal{I}(Z; A)$  using the Barber–Agakov (BA) variational formulation. Starting from

$$\mathcal{I}(Z; A) = \mathcal{H}(A) - \mathcal{H}(A|Z), \quad (19)$$

we introduce a variational conditional density model  $q_\phi(a|z)$  and obtain the lower bound

$$\mathcal{I}(Z; A) \geq \mathcal{H}(A) + \mathbb{E}_{p(z, a)}[\log q_\phi(a|z)]. \quad (20)$$

In practice, we model  $q_\phi(a|z)$  as a conditional diagonal Gaussian with mean predicted by an MLP:

$$q_\phi(a|z) = \mathcal{N}(a; \mu_\phi(z), \text{diag}(\sigma^2)), \quad (21)$$

where  $\mu_\phi(\cdot)$  is an MLP and  $\sigma$  is a global (learned) standard deviation shared across samples. We train  $\phi$  by maximum likelihood on a training split using paired samples  $\{(z_t^{(i)}, a_t^{(i)})\}_{i=1}^N$ . To obtain a plug-in estimate of mutual information in

**Table 5. Latent action entropy on the MI evaluation set.** We compute  $\hat{\mathcal{H}}(Z)$  from the same latent action samples used for KSG MI estimation. Specifically, we treat each quantized latent action vector as a discrete symbol and report its empirical Shannon entropy (in bits). Reporting  $\hat{\mathcal{H}}(Z)$  helps contextualize MI results by showing that the compared models have similar marginal entropy of  $Z$ .

	MVP-LAM	UniVLA	LAPA	Moto
$\hat{\mathcal{H}}(Z)$	$14.16 \pm 0.00$	$13.94 \pm 0.01$	$14.29 \pm 0.00$	$14.28 \pm 0.00$

bits, we also estimate the marginal term  $\mathbb{E}_{p(a)}[\log q(a)]$  using a diagonal Gaussian fitted to the training actions,

$$q(a) = \mathcal{N}(a; \bar{\mu}, \text{diag}(\bar{\sigma}^2)), \quad (22)$$

and report

$$\hat{\mathcal{I}}_{\text{BA}} = \frac{1}{\log 2} (\mathbb{E}_{p(z,a)}[\log q_\phi(a|z)] - \mathbb{E}_{p(a)}[\log q(a)]). \quad (23)$$

We evaluate  $\hat{\mathcal{I}}_{\text{BA}}$  on a held-out test split.

**Protocol and reporting.** For the neural estimators (BA and MINE), we train  $s_\theta$  or  $T_\theta$  on a training split and select the checkpoint based on a validation split (early stopping), then report the final estimate on a disjoint test split. We repeat evaluation across multiple random seeds (which control data subsampling/splitting and optimization randomness) and report the mean and standard deviation. Since different estimators have different biases and scaling, we interpret estimates *within each estimator* and focus on whether the ranking (ours > baseline) is consistent across estimators. Table 4 shows the hyperparameters used in neural estimators. In addition, we report the empirical entropy  $\hat{\mathcal{H}}(Z)$  of each model’s latent actions on the same Bridge V2 subset used for MI estimation (Table 5). This quantifies the diversity of the latent action codes and helps rule out the trivial explanation that differences in MI are driven primarily by different marginal entropies of  $Z$ .

## B.2. Details of Linear Probing

**Training details.** For each dataset, we construct a probing set  $\{(z_t^{(i)}, a_t^{(i)})\}_{i=1}^N$  and train a simple linear layer to predict actions from latent actions. We minimize the mean-squared error:

$$\mathcal{L}_{\text{probe}} = \mathbb{E} \left[ \left\| a_t^{(i)} - \hat{a}_t^{(i)} \right\|_2^2 \right], \quad \hat{a}_t^{(i)} = W z_t^{(i)} + b. \quad (24)$$

As in MI estimation, we freeze the LAM when training the linear probe. Table 4 summarizes the probing hyperparameters.

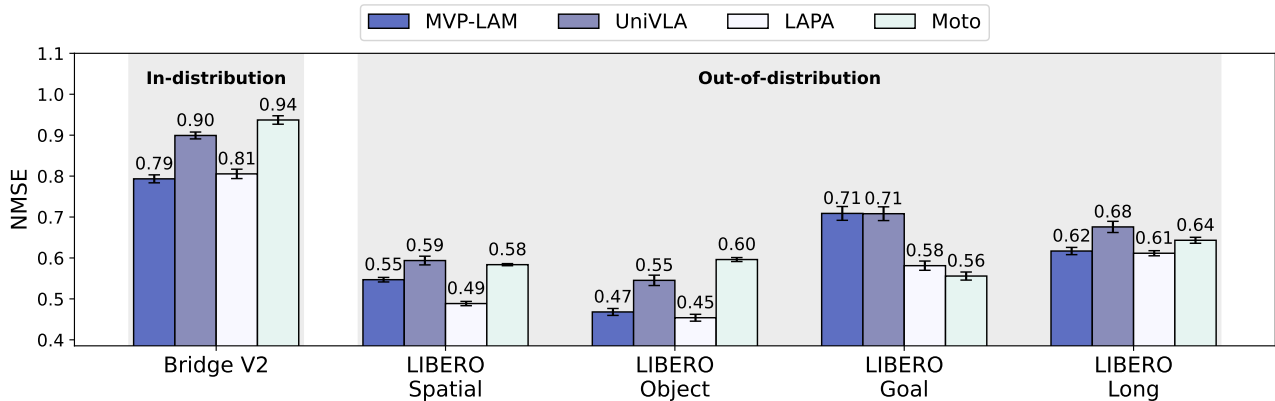


**Figure 7. Extended linear probing.** NMSE of a single linear layer predicting normalized actions from latent actions, evaluated in-distribution (Bridge V2) and out-of-distribution (LIBERO suites). Lower is better. Error bars denote standard deviation over four seeds.

**Extended linear probing results.** Figure 7 reports extended linear probing results including LAPA and Moto. Importantly, MVP-LAM achieves the lowest NMSE on Bridge V2 (in-distribution) among *all* compared methods, including LAPA and

Moto, indicating that its latent actions most directly encode step-level robot control signals on the target training distribution. On LIBERO (OOD), LAPA achieves the lowest NMSE on the Spatial, Object, and Long suites, while Moto performs best on LIBERO-Goal. MVP-LAM is second-best on Spatial, Object, and Long, but underperforms on LIBERO-Goal. This pattern indicates that MVP-LAM yields the most action-predictive latents on Bridge V2, while OOD action predictability can be dominated by additional factors that also affect action-centricity beyond viewpoint robustness alone.

We hypothesize why MVP-LAM struggles in LIBERO OOD evaluation: (i) *data scale*: the multi-view robot subset used for MVP-LAM ( $\sim 55k$ ) is smaller than the training scale used by LAPA ( $\sim 970k$ ) and Moto ( $\sim 109k$ ), which can limit generalization in a purely supervised probe; (ii) *token capacity*: LAPA (larger token dim.) and Moto (larger codebook/longer tokens) have higher-capacity bottlenecks, which can capture more action-relevant signals in OOD distribution; and (iii) *viewpoint distribution*: LIBERO is evaluated from a fixed third-person camera, which may better match dominant viewpoints in pretraining corpora used by LAPA and Moto. We expect OOD action predictability to improve by scaling MVP-LAM with larger multi-view robot datasets (e.g., (Khazatsky et al., 2024; AgiBot-World-Contributors et al., 2025)) and additional multi-view human datasets (e.g., (Zheng et al., 2023; Sener et al.; Kwon et al., 2021)) and by increasing bottleneck capacity (larger codebooks and/or higher-dimensional embeddings). Due to the high computational cost of training LAMs at scale, we leave scaling MVP-LAM to larger multi-view datasets and training larger codebooks as future work.

## C. Details of MVP-LAM

### C.1. MVP-LAM training details

MVP-LAM is trained on a mixture of (i) real-world robot manipulation trajectories and (ii) in-the-wild human manipulation videos. For robot data, we use a subset of Open X-Embodiment (OXE) (Collaboration et al., 2023) that satisfies two conditions: (1) single-arm end-effector control and (2) time-synchronized multi-view trajectories. For human data, we use EgoExo4D (Grauman et al., 2024), which contains  $\sim 5k$  in-the-wild videos with synchronized multi-view recordings.

To match the LfV setting, we do not use proprioceptive inputs or action labels from robot trajectories during MVP-LAM training. Likewise, when using MVP-LAM tokens for VLA pretraining, we only provide visual observations and latent action pseudo-labels. Table 6 lists the datasets and their sampling weights used to train MVP-LAM.

Table 6. **MVP-LAM training mixture.** Datasets and sampling weights used for training MVP-LAM.

MVP-LAM training mixture	
Furniture Bench Dataset	6.58%
Taco Play	7.92%
UTAustin Mutex	6.03%
Berkeley Cable Routing	0.71%
Jaco Play	1.30%
Berkeley Autolab UR5	3.26%
Austin Sirius Dataset	4.66%
Stanford Hydra Dataset	11.93%
IAMLab CMU Pickup Insert	2.44%
NYU Franka Play Dataset	2.24%
Berkeley Fanuc Manipulation	2.09%
Austin Sailor Dataset	5.88%
VIOLA	2.54%
FMB Dataset	18.94%
Austin Buds Dataset	0.57%
Bridge V2	14.79%
EgoExo4D	8.12%

Table 7. **Hyperparameters of MVP-LAM.** Details of training (upper) and model architecture (lower).

Hyperparameters of MVP-LAM	
Batch size	32
Learning rate	$10^{-4}$
Weight Decay	$10^{-2}$
Grad. clip	1.0
VQ beta	0.25
Resolution	224x224
Hidden dim.	768
Patch size	14
Num. Blocks	12

We train MVP-LAM on  $4 \times$  A6000 GPUs. One epoch takes approximately 96 GPU-hours on  $4 \times$  A6000.

## C.2. VLA pretraining and finetuning details

We pretrain a Prismatic-7B VLM (Karamcheti et al., 2024) to predict MVP-LAM latent action tokens with a CE objective, following the UniVLA training recipe. We only use Bridge V2 for VLM pretraining due to limited computational cost. Table 8 summarizes the pretraining hyperparameters. Pretraining is run on  $4 \times$  H200 GPUs, totaling 45 GPU-hours.

Table 8. Hyperparameters used for VLM pretraining with MVP-LAM.

VLM pretraining hyperparameters	
Steps	200k
Learning rate	$2 \times 10^{-5}$
Batch size	96
Max grad norm	1.0

For finetuning, we follow Bu et al. (2025) and train multi-head attention layers that decode the latent action tokens  $z_t$  into continuous robot actions. Specifically, let  $o_t = f(I_t)$  and  $o_{t+1} = f(I_{t+H})$ , and let  $(u_v, u_a)$  denote the vision and latent action embeddings from the final layer of the VLM given  $o_t$ . If the VLM is properly pretrained to predict latent actions, its prediction would be  $z_t = \text{Quantize}(E(o_t, o_{t+1}))$ . We introduce randomly-initialized, learnable query vectors  $q_v$  and  $q_a$ , and apply multi-head attention as

$$u'_v = \mathcal{A}(q_v, u_v, u_v), \quad (25)$$

$$u'_a = \mathcal{A}(q_a + u'_v, u_a, u_a), \quad (26)$$

$$a_{t:t+H} = \text{MLP}(u'_a) \quad (27)$$

where  $\mathcal{A}(Q, K, V)$  denotes a multi-head attention operator with query  $Q$ , keys  $K$ , and values  $V$ . We optimize an  $L_1$  regression loss and a CE loss for the token prediction. Table 9 and 10 show the hyperparameters for finetuning in SIMPLER and LIBERO-Long. We finetune the VLA on  $2 \times$  A6000 GPUs, totaling 18 GPU hours for SIMPLER and 30 hours for LIBERO-Long.

## D. Additional Baseline Details

### D.1. LAM baselines

Table 11 summarizes the discrete bottleneck configurations used by each latent-action model.

**UniVLA** (Bu et al., 2025) learns *task-relevant* latent actions with a two-stage procedure. In Stage 1, it trains a VQ-VAE LAM with language conditioning to obtain a task-agnostic (task-irrelevant) latent action that explains visual transitions. In Stage 2, it freezes the Stage 1 representation and learns an additional latent action representation that captures the remaining, language-related (task-relevant) information. The resulting discrete tokens are then used as pseudo-action labels for VLA pretraining.

**LAPA** (Ye et al., 2024) is one of the first works to use discrete latent actions as pseudo-action labels for VLA pretraining and demonstrates that such tokens can transfer across embodiments. It learns discrete latent actions via VQ-VAE-style transition tokenization and uses the resulting codes as pseudo-actions during pretraining.

**Moto** (Chen et al., 2024b) learns a motion tokenizer that converts videos into longer sequences of discrete motion tokens. It uses a larger codebook ( $K=128$ ) and longer tokenization ( $L=8$ ) with a smaller per-token embedding dimension ( $d=32$ ), resulting in a higher-capacity token sequence for representing motion.

### D.2. Implementation details of baselines

**UniVLA.** For LIBERO-Long finetuning, we reproduce UniVLA using the official code release and follow the released training and evaluation pipeline. We initialize from the VLM checkpoint pretrained on Bridge V2 and finetune for 30k steps with batch size 8 and gradient accumulation 2. Under our setup, the default learning rate  $3.5 \times 10^{-4}$  led to unstable training, so we use  $2.0 \times 10^{-4}$  with a step learning rate schedule. For a fair comparison, we tune only the learning rate for MVP-LAM while keeping all other hyperparameters fixed (Table 10). Note that UniVLA reports 87.5% success on LIBERO-Long in the original paper, which is slightly lower than MVP-LAM’s 90.8%.

**Table 9. VLA finetuning hyperparameters on SIMPLER.** We report optimization settings, action decoder hyperparameters, and LoRA configuration.

VLA finetuning hyperparameters (SIMPLER)	
<i>Training</i>	
Batch size	4
Gradient accumulation	4
Steps	10k
<i>Action decoder</i>	
Learning rate	$10^{-3}$
Weight decay	$10^{-3}$
Window size $H$	5
<i>LoRA</i>	
Rank $r$	32
LoRA $\alpha$	16
Learning rate	$2 \times 10^{-4}$
Weight decay	0.0

**Table 10. VLA finetuning hyperparameters on LIBERO-Long.** We report optimization settings, action decoder hyperparameters, and LoRA configuration.

VLA finetuning hyperparameters (LIBERO-Long)	
<i>Training</i>	
Batch size	8
Gradient accumulation	2
Steps	30k
<i>Action decoder</i>	
Learning rate	$2 \times 10^{-4}$
Weight decay	$10^{-3}$
Window size $H$	12
<i>LoRA</i>	
Rank $r$	32
LoRA $\alpha$	16
Learning rate	$5 \times 10^{-5}$
Weight decay	0.0

**Table 11. LAM configurations.**  $K$  is the codebook size,  $L$  is the number of discrete tokens per transition, and  $d$  is the token embedding dimension.

Model	#Codes ( $K$ )	Code length ( $L$ )	Code dim. ( $d$ )
MVP-LAM	16	4	128
UniVLA	16	4	128
LAPA	8	4	1024
Moto	128	8	32

**Octo.** For both Octo-base and Octo-small, we finetune the language-conditioned policy by updating all parameters (full finetuning) using the official Octo codebase. We finetune for 10k steps with batch size 32 and learning rate of  $3 \times 10^{-4}$ .

$\pi_0$ . For SIMPLER finetuning, we finetune  $\pi_0$  with LoRA using the official codebase, consistent with the other baselines. We finetune for 10k steps with batch size 16 and learning rate  $5 \times 10^{-5}$ . For a fair comparison, we finetune using a single RGB image observation and the language instruction, excluding wrist-view images and proprioceptive inputs.

**Evaluation Details.** We reproduce all baselines *without* the  $\dagger$  mark in Tables 1 and 2. For SIMPLER, we use the values reported in Ye et al. (2024) for LAPA and OpenVLA. For LIBERO-Long, we use the values reported in Kim et al. (2024) for OpenVLA, Bu et al. (2025) for UniVLA (OXE), and Kim et al. (2025b) for  $\pi_0$ . Training recipes for LIBERO-Long vary across works; therefore, these reported values should be treated as reference numbers rather than directly comparable results.

## E. Additional Visualization

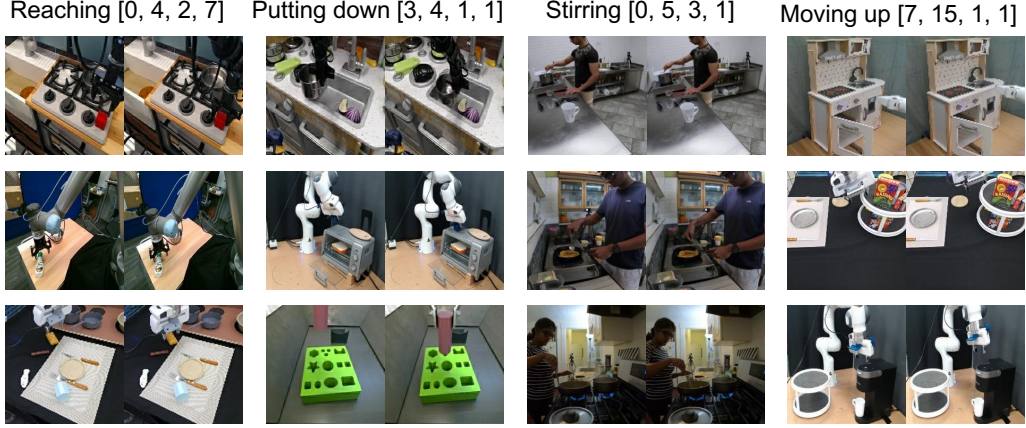
### E.1. Latent action examples

Figure 8 visualizes example latent action tokens produced by MVP-LAM for representative frame transitions. We display the discrete codes selected for each transition, along with the corresponding before/after observations. Across examples from different sources, similar motion patterns tend to activate similar codes, illustrating how MVP-LAM clusters transition dynamics in a shared token space without using action supervision.

### E.2. Result of novel view synthesis in Bridge V2

To evaluate the viewpoint robustness of LAM, we use a zero-shot novel view synthesis (NVS) model finetuned from DROID dataset (Tian et al., 2024). Due to the computational cost of zero-shot novel view synthesis, we use a subset of Bridge V2. We first sample 100 trajectories from Bridge V2 and synthesize 5 perturbed images for each step, totaling 3.7k viewpoint-perturbed transition samples. Given an initial camera pose  $(\mathbf{p}_0, \mathbf{q}_0)$ , where  $\mathbf{p}_0 \in \mathbb{R}^3$  denotes the camera position and  $\mathbf{q}_0 \in \mathbb{R}^4$  denotes the camera orientation as a unit quaternion, we sample  $N = 5$  perturbed poses by independently

**Figure 8. Qualitative latent action visualization.** Example frame transitions and the corresponding MVP-LAM discrete codes selected for each transition.



applying Gaussian noise to translation and rotation:

$$\Delta\theta \sim \mathcal{N}(\mathbf{0}, \sigma_\theta^2 \mathbf{I}), \quad \Delta\mathbf{p} \sim \mathcal{N}(\mathbf{0}, \sigma_p^2 \mathbf{I}), \quad (28)$$

where  $\Delta\theta$  is a small rotation in axis-angle representation and  $\Delta\mathbf{p}$  is a 3D translation. We construct the perturbed pose as  $\mathbf{p} = \mathbf{p}_0 + \Delta\mathbf{p}$  and  $\mathbf{q} = \Delta\mathbf{q} \otimes \mathbf{q}_0$ , where  $\Delta\mathbf{q}$  is the unit quaternion converted from  $\Delta\theta$  and  $\otimes$  denotes quaternion multiplication. Unless otherwise specified, we use  $\sigma_\theta = 0.075$  rad and  $\sigma_p = 0.03$  m. We summarize the sampling hyperparameters of the NVS model in Table 12.

**Table 12. NVS sampling hyperparameters.** We use DDIM sampling with the following configuration for novel-view synthesis.

Hyperparameters of NVS model	
DDIM steps	250
DDIM $\eta$	1.0
Precomputed scale	0.6
Field of view	70°

### E.3. Additional analysis of viewpoint perturbation of LAPA and Moto

A potential concern with Figure 6 is that measuring errors in the DINOv2 feature space could disadvantage pixel-decoding LAMs, since their predictions must be re-embedded before computing MSE. To probe this, we additionally evaluate pixel-level reconstruction quality for LAPA and Moto, which explicitly decode RGB frames.

**Table 13. Pixel-level prediction quality under viewpoint perturbations.** PSNR measures reconstruction quality on unperturbed transitions.  $\widetilde{\text{PSNR}}$  measures reconstruction quality when the latent action is inferred from a viewpoint-perturbed transition. Results are reported as mean $\pm$ std over 3 random seeds.

Models	PSNR $\uparrow$	$\widetilde{\text{PSNR}} \uparrow$
LAPA	$21.04 \pm 0.01$	$14.91 \pm 0.01$
Moto	$23.87 \pm 0.00$	$13.02 \pm 0.02$

Table 13 reports PSNR on unperturbed transitions and  $\widetilde{\text{PSNR}}$  when the latent action is inferred from a viewpoint-perturbed transition. Both methods exhibit a substantial degradation under perturbation, indicating that their failures are already apparent at the pixel level, rather than being an artifact of re-embedding into DINOv2. Qualitative results in Fig. 9 further support this: while predictions remain relatively coherent on the original view, the perturbed setting often produces severely blurred or distorted frames that no longer preserve the scene structure.

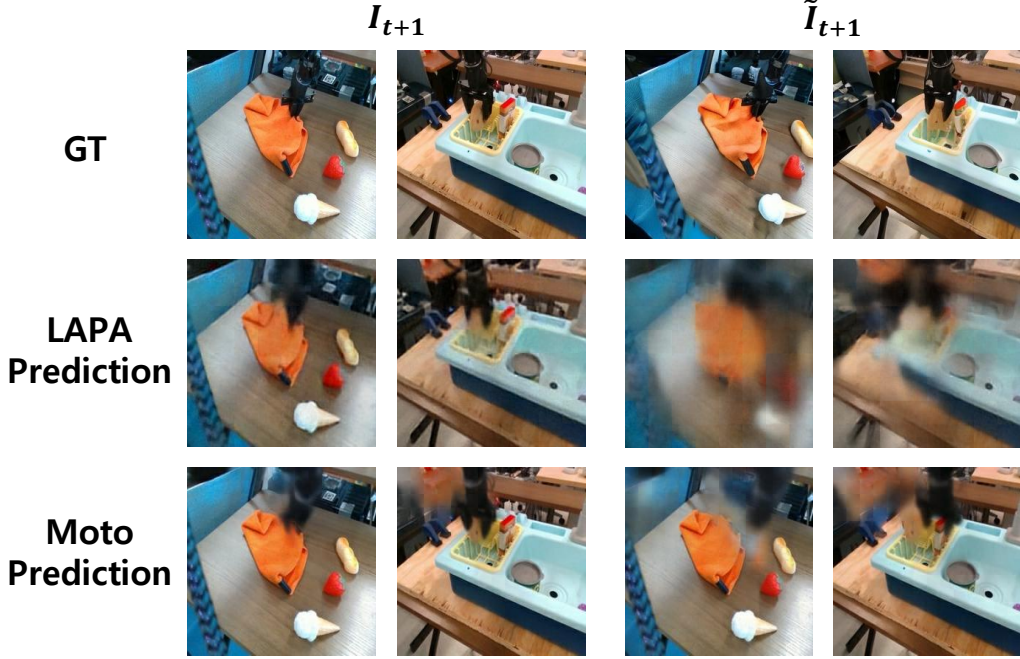


**Figure 9. Qualitative reconstructions under viewpoint-perturbed latent actions inference.** Predicted next frames from LAPA and Moto on Bridge V2. While predictions are relatively coherent on unperturbed inputs (left), inferring the latent action from a viewpoint-perturbed transition (right) often leads to visibly degraded reconstructions, consistent with the drop in  $\widetilde{\text{PSNR}}$ .

This analysis suggests that the higher DINOv2-space errors for pixel-decoding LAMs are consistent with a genuine drop in sample quality under viewpoint-perturbed latent-action inference. At the same time, our models do not decode pixels, so we cannot perform a perfectly symmetric pixel-metric comparison (e.g., PSNR for MVP-LAM). We therefore use DINOv2-space prediction error as a common evaluation space across all methods, and provide the pixel-level results above as supporting evidence that the observed gap is not solely due to the choice of feature-space metric.